RSC Advances

PAPER

View Article Online
View Journal | View Issue

Cite this: *RSC Adv.*, 2015, **5**, 49385

Co_3O_4 nanoparticles/cellulose nanowhiskers-derived amorphous carbon nanoneedles: sustainable materials for supercapacitors and oxygen reduction electrocatalysis†

R. Silva,[a] G. M. Pereira,[a] D. Voiry,[b] M. Chhowalla[b] and T. Asefa*[cd]

Received 1st May 2015
Accepted 26th May 2015

DOI: 10.1039/c5ra08037a

www.rsc.org/advances

Hybrid nanostructured materials comprised of amorphous carbon nanoneedles (CNN)-supported Co_3O_4 nanoparticles (Co_3O_4-CNN) were synthesized. The synthesis involved layer-by-layer nanocasting of cellulose nanowhiskers with precursors of cobalt oxide and silica, followed by pyrolysis of the core–shell–shell composite materials and etching of the outer silica shells from the carbonized materials. Notably, cotton-derived cellulose nanowhiskers were used as the carbon precursors, and also as the hard templates for needle-shaped carbons, in the synthesis. The effectiveness of the core–shell–shell nanoreactors, possessing the silica shell-entrapped cellulose nanowhiskers and Co(II) ions, in generating organized carbon nanomaterials with metal oxide nanoparticles, or otherwise, as a function of the loading of Co(II) ions was evaluated. Details of the synthetic method and the different materials in terms of composition and morphology it results in as a function of the relative amount of metal ions have also been discussed. The materials showed promising supercapacitive properties and electrocatalytic activity for the oxygen reduction reaction (ORR). The materials' double layer capacitance and performance for ORR electrocatalysis as a function of their Co_3O_4 content and particles size have also been discussed. The results indicated that the electrochemical properties of these hybrid materials are strongly related to the morphology of their carbon nanostructures. The synthetic method demonstrated here can potentially serve as a facile route to produce other metal oxide/carbon nanomaterials, with different morphologies and similar or better properties, using other carbon precursors.

Introduction

Fuel cells allow the energy stored in chemical form in sustainable energy sources such as hydrogen to be recovered as electrical energy at/or near ambient temperature.[1,2] However, in many conventional and commercially available fuel cells the cathode and anode electrodes contain electrocatalysts composed of expensive and less earth abundant noble metals such as platinum.[3] And, the relative low earth abundance and high cost of such noble metals has long posed serious concerns on the feasibility of fuel cell technologies for large scale uses. Additionally, even with such expensive electrocatalysts, a great portion of the energy in fuel cells is lost due to the large overpotential needed to overcome the oxygen reduction reaction (ORR) at the cathodic half-reaction of fuel cells (as the ORR typically requires overpotentials as high as 500–600 mV to take place even with platinum-based catalysts).[4] The severe activation loss associated with ORR, coupled with the intrinsic low kinetics of the reaction, is therefore often responsible for the limited current density as well as cell voltage given off by many conventional fuel cells.[5,6]

Hence, breakthrough technological advances in fuel cells demand the development of sustainable, noble metal-free, alternative electrocatalysts to platinum, and those that can catalyze ORR with at least the same efficiency as,[7] if not better than, platinum.[8] It is only then that the large scale deployment of fuel cells based on energy sources such as hydrogen to meet the so-called "hydrogen economy" can be realized.[9]

To this end, intensive research in this area has recently led to various ORR electrocatalysts that contain inexpensive and earth-abundant early transition metals.[10,11] In particular, cobalt and cobalt oxides supported on carbon materials, especially graphene, have emerged as viable alternatives to conventional

[a]*Departamento de Química, Universidade Estadual de Maringá, Avenida Colombo 5790, CEP: 87020-900-Maringá, Paraná, Brazil*

[b]*Department of Materials Science and Engineering, Rutgers, The State University of New Jersey, 607 Taylor Road, Piscataway, New Jersey 08854, USA*

[c]*Department of Chemistry and Chemical Biology, Rutgers, The State University of New Jersey, 610 Taylor Road, Piscataway, New Jersey 08854, USA. E-mail: tasefa@rci.rutgers.edu*

[d]*Department of Chemical and Biochemical Engineering, Rutgers, The State University of New Jersey, 98 Brett Road, Piscataway, New Jersey 08854, USA*

† Electronic supplementary information (ESI) available. See DOI: 10.1039/c5ra08037a

Pt/C electrocatalysts.[12–14] This is because supported cobalt or cobalt oxides can catalyze ORR effectively while cobalt meets the requirements of sustainable materials due to its relatively high earth-abundance, low cost (which is only a fraction of that of platinum), and low toxicity especially compared with many other heavy metals.[15]

On the other hand, owing to its conducive electronic properties for electrochemical processes, graphene has been widely considered as a support material for many metallic- and metal oxide-based nanoparticles for electrocatalysis.[16,17] However, the potential use of graphene and its derivatives as a support material for electrocatalysts has some limitations too, with the most notable of which being the unavailability of synthetic methods that can produce pristine graphene on large scale for scalable production of such electrocatalysts. This also explains why despite reports of a number of graphene-based electrocatalysts, many of them in actuality contain either graphene oxide (GO) or reduced graphene oxide (rGO), and not pristine graphene.[18,19] Unlike pristine graphene, which has no band gap, GO and rGO are indirect band gap materials with substantially different electronic properties.[20] This is merely due to the presence of hydrogen and oxygen moieties (or impurities) on the latter. Nevertheless, besides substantially changing the carbon material's inherent properties, the presence of such 'impurity', even in tiny amount, on carbonaceous materials such as graphene affects the surface interactions and charge transfers between the carbon support materials and the supported nanoparticles, and thereby the overall materials' potential applications in areas such as (electro)catalysis and charge storage.[21,22]

Therefore, other viable support materials, alternative to graphene but still allow cobalt-based electroactive moieties to transfer their charges easily and give enhanced electrocatalytic activity toward ORR, are highly desired. In view of this and the issues mentioned above, we had thought that the nanoreactor method we had previously used to make pure crystalline carbon nanoneedles[23] could be exploited to produce carbon nanoneedle (CNN)-supported early transition metal oxide nanoparticles for electrocatalysis (*i.e.*, unique types of carbon nanomaterials with high proportions of plane edges and good electrical conductivity decorated with electrocatalytic active metal oxides on their surfaces). Herein this synthetic idea is shown to work, with the report of the synthesis of carbon nanoneedles-supported cobalt oxide electrocatalysts, as illustrated in Fig. 1, that exhibit good electrocatalytic activity for ORR. Moreover, the ability of the materials to serve as high performance supercapacitors is also demonstrated.

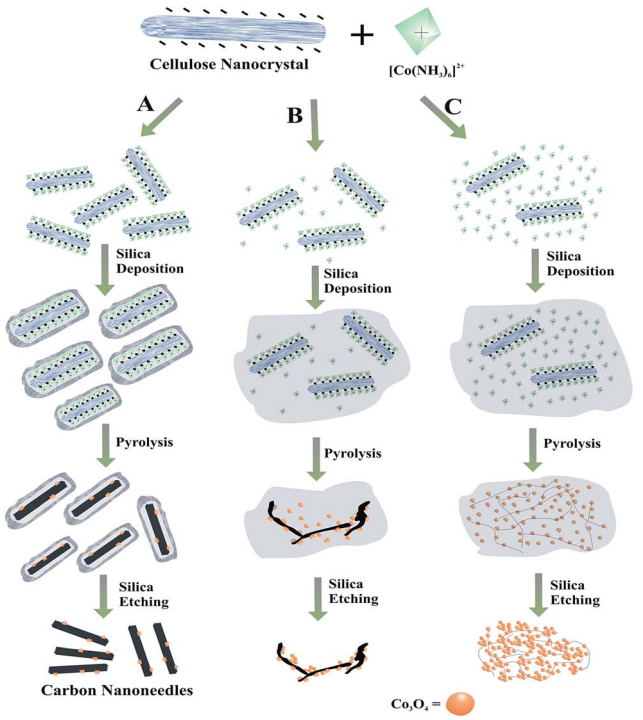

Fig. 1 Schematic representation of the synthetic route used to make cellulose-derived amorphous carbon nanoneedles-supported Co_3O_4 nanoparticles (denoted as Co_3O_4/CNN) with different structures and compositions. The synthesis involved: (1) preparation of cellulose nanowhiskers, (2) functionalization of the surfaces of cellulose nanowhiskers with solutions of $[Co(NH_3)_6]^{2+}$ ions with different relative concentrations, (3) deposition of silica shells around the $[Co(NH_3)_6]^{2+}$-modified cellulose nanowhiskers, and (4) pyrolysis of the resulting Co^{2+}/cellulose@SiO_2 core–shell nanowhiskers, and (5) finally etching of the silica shells from the carbonized Co_3O_4/CNN@SiO_2 material. The three different concentrations of $[Co(NH_3)_6]^{2+}$ ions used for the synthesis of the materials led to three different Co_3O_4/CNN materials with different structures and amounts of Co_3O_4, namely: sample Co_3O_4/CNN-A with lower amount of Co_3O_4 compared with carbon, Co_3O_4/CNN-B with comparable amounts of Co_3O_4 and carbon (almost 1 : 1 ratio by weight), and sample Co_3O_4/CNN-C with larger amount of Co_3O_4 than carbon by weight.

Results and discussion

Materials synthesis and characterization

The first step in the synthesis of the Co_3O_4/CNN materials involved the successive encapsulation of nanostructured carbon precursors derived from a natural source with metal complexes, followed by thermally robust silica shells (or nanocages). Specifically, cellulose nanowhiskers prepared by acid hydrolysis from cotton were coated by hexaamminecobalt(II) complex ($[Co(NH_3)_6]^{2+}$) and then by silica shells, both *via* electrostatic self-assembly, as schematically shown in Fig. 1. The resulting Co^{2+}/cellulose@SiO_2 core@shell nanomaterials were treated at high temperature under inert atmosphere (N_2) in different stages as presented in Fig. S1.† This allowed the cellulose nanowhiskers trapped inside the nanocages to undergo carbonization and form carbon nanoneedles with shapes akin to the shapes of the nanocages. At the same time, the metal complexes sandwiched between the cellulose cores and the silica shells were thermally transformed into metal oxide nanoparticles. Upon removal of the silica shells, freestanding carbon nanoneedles decorated with Co_3O_4 nanoparticles (Co_3O_4/CNN) that can efficiently electrocatalyze ORR and effectively store charges were obtained. Although we used this type of synthetic method to produce *crystalline* carbon nanoneedles before,[23] it is in this present work that the method is shown, for the first time, to be applicable for making amorphous carbon nanoneedles-supported early transition metal

oxides *in situ*. Moreover, it is also for the first time that materials synthesized this way are shown to have high electrocatalytic activity for ORR as well as good charge storage capacity.

Besides serving as precursor for the desired metal oxide catalytic sites (*i.e.*, Co_3O_4 nanoparticles, in this case), the metal complexes ($[Co(NH_3)_6]^{2+}$) anchored onto the cellulose nanowhiskers play two more important roles. First, they allow the formation of silica shells around the cellulose nanowhiskers, by enabling the spontaneous electrostatic deposition on the surfaces of the cellulose nanowhiskers of negatively charged silicate intermediates formed from the hydrolysis and condensation silica precursors under basic conditions. Second, they serve as catalyst, promoting the formation of graphitic carbon during the carbonization step (please note that metallic phases composed of Fe, Cu and Ni are well-known to promote graphitization of carbon during high temperature carbonization processes[24]).

Specifically, as depicted in Fig. 1, three different concentrations (*i.e.*, relatively low, moderate or high) of $[Co(NH_3)_6]^{2+}$ were used in the synthesis, which after carbonization led to three Co_3O_4/CNN@SiO_2 materials, labeled as Co_3O_4/CNN@SiO_2-A, -B and -C, respectively. After removal of the silica shells, three different Co_3O_4/CNN materials, denoted as Co_3O_4/CNN-A, Co_3O_4/CNN-B and Co_3O_4/CNN-C, respectively, with less, moderate and large relative amount Co_3O_4, respectively, were ultimately obtained, as discussed in more detail below.

The structure and composition of the resulting Co_3O_4/CNN materials were then characterized by different analytical techniques. Fig. 2 displays the powder X-ray diffraction (XRD) patterns of Co_3O_4/CNN@SiO_2-A and Co_3O_4/CNN@SiO_2-B. In the XRD pattern of Co_3O_4/CNN@SiO_2-A (which was synthesized with the lowest amount of $[Co(NH_3)_6]^{2+}$ ions), no visible well-defined peaks corresponding to crystalline phases are observed. The result suggests that the Co_3O_4 on this material, whose presence is confirmed by other methods (*vide infra*), are either too small in size or in amount, or are inherently amorphous to diffract X-ray beams. On the other hand, the diffraction pattern of Co_3O_4/CNN@SiO_2-B clearly displays peaks that correspond to Co_3O_4. Nevertheless, the diffraction peaks are still broad in the latter case, suggesting that the Co_3O_4 particles formed in Co_3O_4/CNN@SiO_2-B are small in size.

The relative amount of Co_3O_4 in the Co_3O_4/CNN materials was determined by thermogravimetric analysis (TGA) under a flow of synthetic air (20% O_2 in N_2). The TGA results are presented in Fig. 3. From the residual weight obtained after the complete decomposition of the composite materials under synthetic air, the content of Co_3O_4 in each material was then determined. Accordingly, the relative amount of Co_3O_4 in Co_3O_4/CNN@SiO_2-A, -B and -C were found to be 6.4, 57.5, and 81.4%, respectively. This also means that Co_3O_4/CNN-A has the least amount of Co_3O_4 (*ca.* 6%) by weight with respect to carbon, Co_3O_4/CNN-B contains comparable weight ratio of Co_3O_4 and carbon, and Co_3O_4/CNN-C has the highest relative amount of Co_3O_4 (*ca.* 81%) with respect to carbon. The result also clearly indicates the broadly varying composition or content of Co_3O_4 in the materials, as a result of a simple change in the relative amount of $[Co(NH_3)_6]^{2+}$ complex used for the synthesis of the materials.

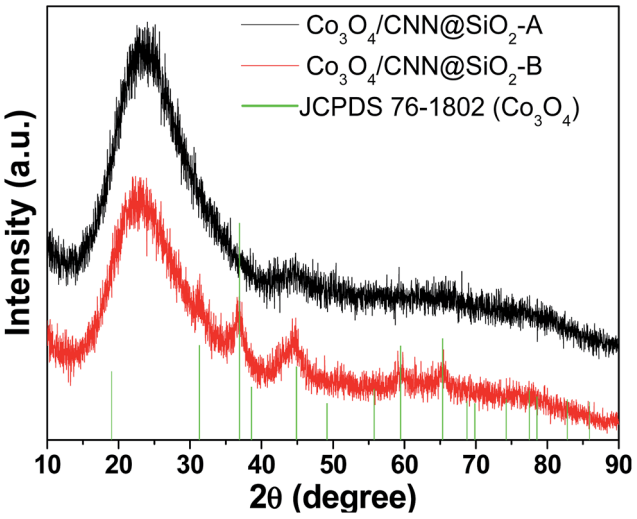

Fig. 2 XRD patterns of Co_3O_4/CNN@SiO_2-A and Co_3O_4/CNN@SiO_2-B.

The morphologies of the Co_3O_4/CNN materials were probed by TEM microscopy, and the results are displayed in Fig. 4. The TEM images generally suggest that the amount of $[Co(NH_3)_6]^{2+}$ used in the synthesis also significantly affects the morphology of the final materials, besides their compositions or relative amounts of Co_3O_4 as discussed above. The TEM image of Co_3O_4/CNN@SiO_2-A (Fig. 4a) shows the presence of needle-shaped nanostructures. Under higher magnification, the TEM image (Fig. 4b) further shows the presence of Co_3O_4 nanoparticles with *ca.* 8–10 nm in diameter.

On the other hand, no needle-shaped carbon nanostructures were observed in the TEM images of Co_3O_4/CNN@SiO_2-B and Co_3O_4/CNN@SiO_2-C (Fig. 4c–e). The TEM images of Co_3O_4/CNN@SiO_2-B rather show the presence of large numbers of Co_3O_4 nanoparticles with an average size of *ca.* 10 nm

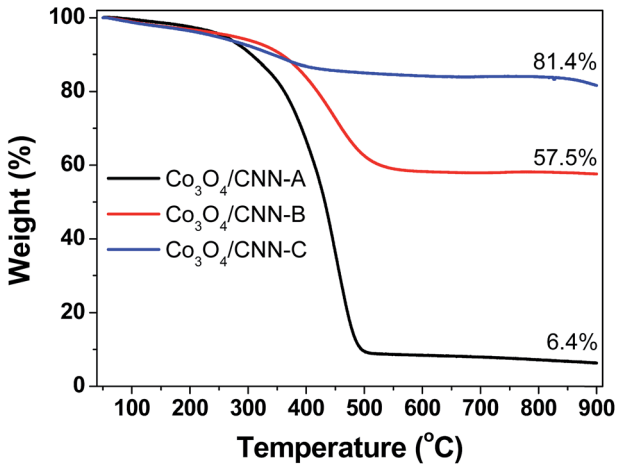

Fig. 3 Thermogravimetric traces obtained for the different Co_3O_4/CNN materials at a heating rate of 10 °C min^{-1} under a constant flow of synthetic air (20% O_2 in N_2) at a rate of 20 mL min^{-1}.

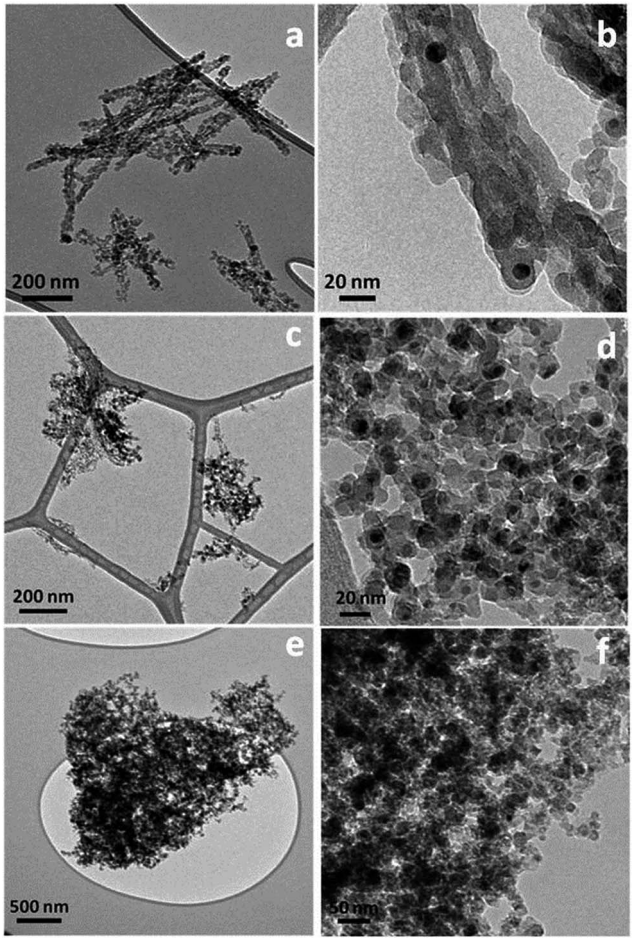

Fig. 4 TEM images of Co_3O_4/CNN@SiO_2-A (a and b), Co_3O_4/CNN@SiO_2-B (c and d), and Co_3O_4/CNN@SiO_2-C (e and f).

distributed over highly interconnected carbon nanostructures (Fig. 4d). On the other hand, despite the TEM images of Co_3O_4/CNN@SiO_2-C (Fig. 4e and f) also show small nanoparticles (10–20 nm), the nanoparticles are highly interconnected or aggregated, reaching sizes up to few micrometers. This is most likely to do with the relatively high amount of $[Co(NH_3)_6]^{2+}$ ions used for the synthesis of this particular material, compared with those used to make the other two materials. In fact, this material had 81.4% Co_3O_4 by weight, or conversely relatively little carbon.

Supercapacitive properties of Co_3O_4/CNN materials

Next, the specific capacitance of the Co_3O_4/CNN materials was measured with cyclic voltammetry (Fig. 5). Using the results, the relationship between the specific capacitance and the structure/morphology of the materials was also elucidated. All the electrochemical measurements were carried out using a saturated calomel electrode (SCE) as reference, which was converted to reversible hydrogen electrode (RHE) as described in ESI and Fig. S2.†

As the Co_3O_4/CNN materials obtained by using different concentrations of $[Co(NH_3)_6]^{2+}$ were found to possess different

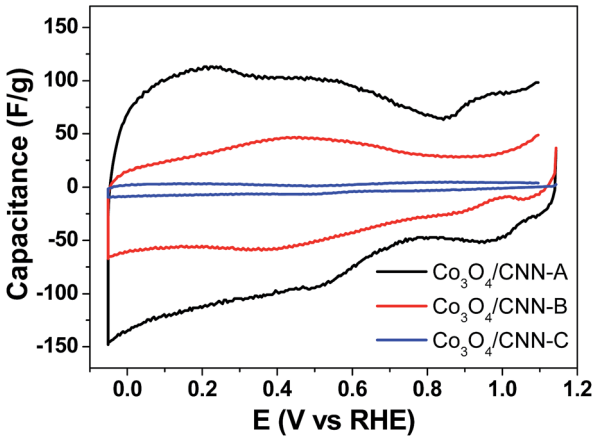

Fig. 5 Specific capacitance *versus* applied potential (*E vs.* RHE) in 0.1 M KOH measured by cyclic voltammetry for Co_3O_4/CNN materials supported on a 5 mm in diameter glassy carbon working electrode with a loading of 100 μg cm^{-2}. The cyclic voltammograms were collected at scan rate of 20 mV s^{-1}.

amounts of Co_3O_4 and have distinct structures, they were expected to exhibit different charge storage capacity as well. Moreover, as the electrochemical capacitance of carbonaceous materials like Co_3O_4/CNN often stems from the electrical double-layers forming on the surfaces of the materials, the capacitance (C) of the materials can be directly correlated to the electrochemical specific surface areas of the materials, with eqn (1):[25]

$$C = \frac{\varepsilon A}{d} \quad (1)$$

where ε is the electrolyte dielectric constant, A the surface area accessible to ions, and d the distance between the center of the ion and the surface of the sample. By using the results, insights into the relationships between the structures of the Co_3O_4/CNN materials and their accessible electrochemical surface areas could then be gleaned.

In Fig. 5, the graphs of electrochemical capacitance *versus* potential for the three materials are presented. The values of specific capacitance in the potential range of −0.05 to 1.15 V *vs.* RHE were found to be 90.8, 33.6, and 3.1 F g^{-1} for Co_3O_4/CNN-A, Co_3O_4/CNN-B, and Co_3O_4/CNN-C, respectively. The result clearly shows that the three materials have significantly different capacitance. The result also shows a very clear inverse relationship between the capacitance of the materials and the amount of Co_3O_4 they contain. The lowest capacitance was found for Co_3O_4/CNN-C, which has a large density of highly aggregated clusters of Co_3O_4 nanoparticles with 10–20 nm in size, whereas the highest specific capacitance was obtained for Co_3O_4/CNN-A, which has needle-shaped nanostructured carbon with relatively small amount of Co_3O_4 with *ca.* 8–10 nm in size. Although needle-like structures are also verified in sample B by TEM, the specific capacitance of Co_3O_4/CNN-B, which is composed of 57.5% of Co_3O_4, is 3-fold lower than that of Co_3O_4/CNN-A, which has only 6.4% of Co_3O_4. Consequently, it can be fairly concluded that Co_3O_4/CNN-A' relatively high amount of carbon and needle-shaped nanostructures, which can provide

the material with large electrochemical active surface area, are responsible for Co_3O_4/CNN-A's high double layer capacitance.

Electrocatalytic properties of Co_3O_4/CNN materials for ORR

The electrocatalytic properties of all the Co_3O_4/CNN materials toward ORR were then tested, and by using the results the interplay between the composition/structural features and the electrocatalytic activities of the materials was probed. To quickly check if the Co_3O_4/CNN materials can catalyze ORR, cyclic voltammogram (CV) over Co_3O_4/CNN-A in O_2-saturated, 0.1 M KOH solution was first performed (Fig. 6). As a negative control, the cyclic voltammogram (CV) of the same material in N_2-saturated KOH solution (0.1 M) was also conducted, and the result was included (Fig. 6). When comparing the two curves, a strong catalytic reduction peak over Co_3O_4/CNN-A (with an onset potential of 0.81 V *vs.* RHE) is seen in the curve obtained under the O_2-saturated solution. Conversely, no such reduction peak is observed for the one obtained in the N_2-saturated solution. These results clearly indicate that Co_3O_4/CNN-A effectively catalyzes the ORR.

In Fig. 7 the CVs of all the three Co_3O_4/CNN materials obtained in O_2-saturated KOH solution (0.1 M) are shown together. From the graphs, all the three materials, Co_3O_4/CNN-A, -B, and -C can be seen to electrocatalyze ORR, with onset potentials of 0.81 V *vs.* RHE, 0.82 V *vs.* RHE and 0.68 V *vs.* RHE, respectively. So, among the three materials, Co_3O_4/CNN-C can be said to have the highest overpotential or the lowest electrocatalytic activity toward ORR, despite its highest amount of Co_3O_4. On the other hand, Co_3O_4/CNN-A and Co_3O_4/CNN-B show lower overpotentials and better electrocatalytic activity toward ORR. It is also interestingly to note that the catalytic activity of Co_3O_4/CNN-A is similar to that of Co_3O_4/CNN-B, despite the former contains approximately 10-fold lower amount of Co_3O_4 than the latter. Moreover, when the activities of the materials towards ORR are compared based on current density, it can be seen Co_3O_4/CNN-A is once again a better electrocatalyst than either Co_3O_4/CNN-B or Co_3O_4/CNN-C. So,

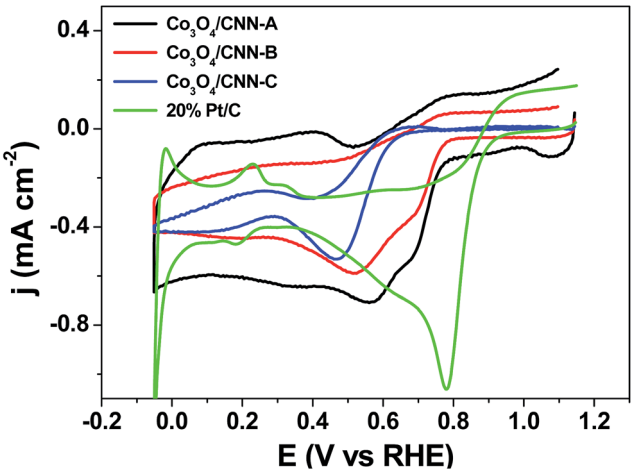

Fig. 7 Cyclic voltammograms of Co_3O_4/CNN-A, Co_3O_4/CNN-B, and Co_3O_4/CNN-C in O_2 saturated KOH solutions (0.1 M) at scan rate of 20 mV s^{-1}.

these results indicate that the difference in electrocatalytic activity between these three materials can be attributed to their carbon nanostructures and the relative amount of carbon materials they contain. It is worth reiterating here again that the former is composed of a large amount of, needle-shaped carbon nanostructures while the latter two possess relatively less amount of carbon with disorganized nanostructures. Similarly, Co_3O_4/CNN-B contains relatively larger amount of carbon materials compared with Co_3O_4/CNN-C. These said, it is worth adding here that CNN material made without Co_3O_4 or by using a small amount $FeCl_3$, which was added only to promote the formation of needle-shaped carbons for the synthesis of CNN, did show significantly lower activity than Co_3O_4/CNN-A, with onset potential of 0.67 V *vs.* RHE (Fig. S3†). So, overall, besides the needle-shaped carbon nanostructures, the presence of some optimal amount of Co species (and Co_3O_4 nanoparticles) directly or indirectly assists the material with its electrocatalytic

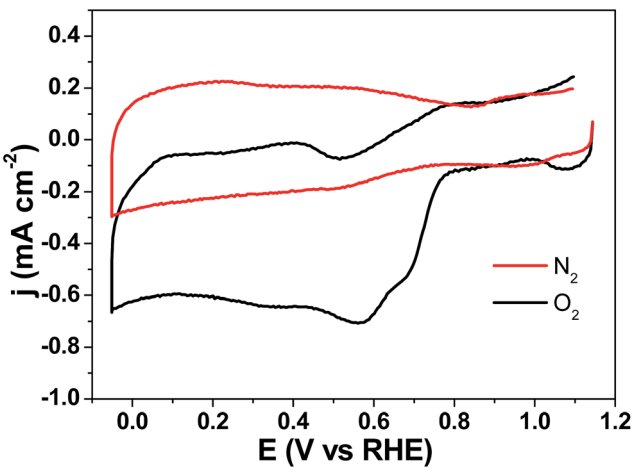

Fig. 6 Cyclic voltammograms over Co_3O_4/CNN-A in O_2- and N_2-saturated KOH (0.1 M) solutions at scan rate of 20 mV s^{-1}.

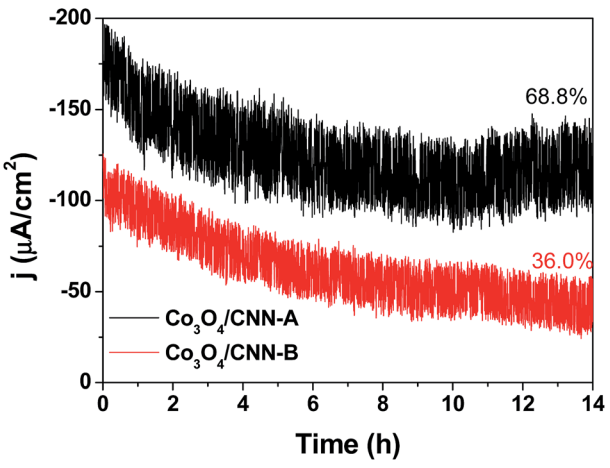

Fig. 8 Chronoamperometric curves ORR over Co_3O_4/CNN-A and Co_3O_4/CNN-B in O_2-saturated KOH solution (0.1 M) at constant potential of 0.73 V *vs.* RHE.

activity toward ORR. This is most likely why Co_3O_4/CNN-A showed the best electrocatalytic activity for ORR compared with the materials we have investigated here. It is worth adding here that the electrocatalytic activity of Co_3O_4/CNN-A is also actually comparable to that of some of the most efficient graphene and carbon nanotube-supported Co_3O_4 materials reported previously, albeit it is lower than that of Pt/C (20%) (Fig. 7).[26]

The stability of Co_3O_4/CNN-A and Co_3O_4/CNN-B during ORR were tested with chronoamperometry for a period of 14 h at constant applied potential of 0.73 V *vs.* RHE (Fig. 8). In the chronoamperometric curve of Co_3O_4/CNN-A, the current density is seen to decrease slightly over 9 h of direct use, but remains stable afterwards. At the end of the experiment, while the current density of Co_3O_4/CNN-A reaches *ca.* 68.8% of the initial value, that of Co_3O_4/CNN-B decreases continuously and reaches as low as 36% of the initial value after 14 h of direct use. So, the results show that compared with Co_3O_4/CNN-B, Co_3O_4/CNN-A not only gives higher current density but also retains the higher current density over longer time period. This huge difference between Co_3O_4/CNN-A and Co_3O_4/CNN-B and Co_3O_4/CNN-A's more stability as electrocatalyst in ORR further highlights the benefits of the carbon nanoneedle structures and the optimal density of Co_3O_4 in it for electrocatalysis.

Finally, polarization curves were obtained for the ORR over Co_3O_4/CNN-A electrocatalyst at different spin rates on a rotating disk electrode (RDE), and the results are presented in Fig. 9A. The corresponding Koutecky–Levich plots obtained from the polarization curves (Fig. 9B) indicate that the average number of electron transferred in the range of 0.07 to 0.56 V *vs.* RHE is 2.22. This suggests the high selectivity of Co_3O_4/CNN-A electrocatalysts for 2-electron process in ORR, which favors the formation of hydrogen peroxide from the reduction of O_2.[8]

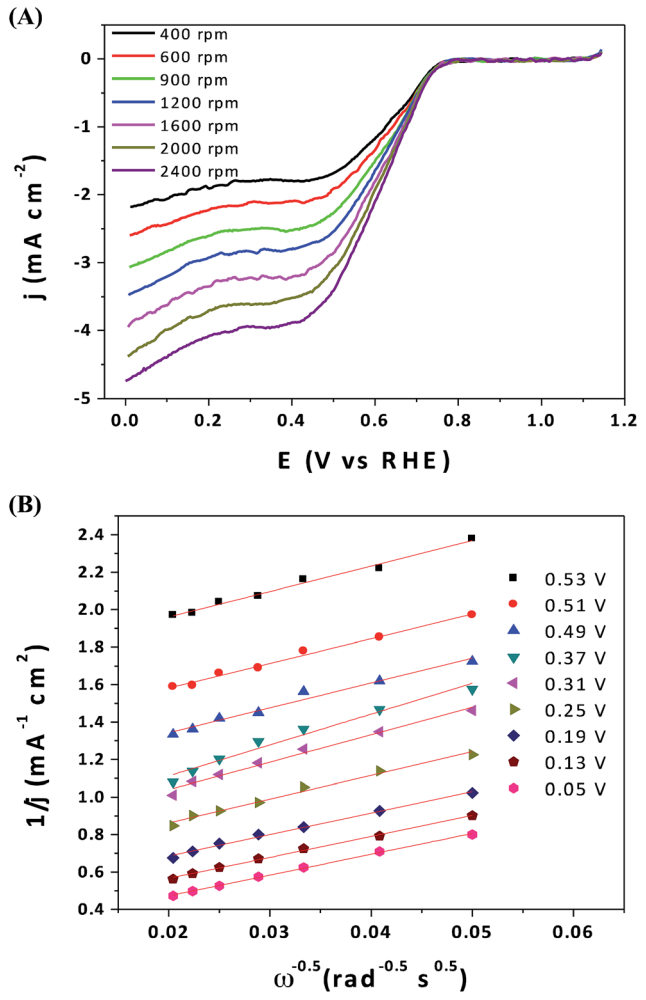

Fig. 9 (a) RDE steady-state polarization curves for the ORR on the Co_3O_4/CNN-A catalyst in O_2-saturated KOH (0.1 M) solution at various rotating rates, as indicated next to the curves (in rpm), and (b) the Koutecky–Levich plots for the ORR over Co_3O_4/CNN-A materials that was used as electrocatalyst at different electrode potentials.

Conclusions

The synthesis of carbon nanoneedles-supported Co_3O_4 nanoparticles with different amount of Co_3O_4 nanoparticles using cotton-derived cellulose nanowhiskers as precursors has been described. The materials have been shown to have high supercapacitive charge storage properties as well as efficient catalytic activities for ORR. Specifically, three different materials containing amorphous carbon nanoneedles with relatively low (6.4%), moderate (57.5%), and high (81.4%) amount of Co_3O_4, denoted as Co_3O_4/CNN-A, Co_3O_4/CNN-B, and Co_3O_4/CNN-C, respectively, have been synthesized and characterized by various analytical methods. While Co_3O_4/CNN-B and Co_3O_4/CNN-C showed disorganized structure, Co_3O_4/CNN-A showed well-defined carbon nanoneedles decorated with Co_3O_4 nanoparticles, as characterized by TEM and XRD. Their XRD patterns, on the other hand, have indicated that the carbon phases in the materials are amorphous. Among the samples investigated here, Co_3O_4/CNN-A has afforded a high specific capacitance, which is attributed to its nanoneedle morphology, and most importantly, its high electrochemical active surface area. The results have also clearly revealed the trends between the electrochemical capacitance and the structures of the materials or the size of Co_3O_4 nanoparticles they contain. Co_3O_4/CNN-A has also exhibited the highest catalytic activity for ORR, in terms of overpotential, current density and stability. The electrocatalytic activity of these amorphous carbon nanoneedles-supported Co_3O_4 nanoparticles, especially of Co_3O_4/CNN, has been found to be comparable with some of the most efficient graphene and carbon nanotube-supported Co_3O_4 nanomaterials reported previously.[26] The results suggested that the structures of the underlying carbon needle support materials and the presence of optimal amount of Co_3O_4 nanoparticles play outstanding roles in the Co_3O_4/CNN-A's catalytic activities toward ORR.

Experimental

Synthesis of cellulose nanowhiskers

To synthesize cellulose nanowhiskers, cotton (6 g) was taken and soaked in aqueous NaOH (1 M) solution (300 mL) for 1 h. The cotton was then removed from the solution and washed

with copious amount of distilled water and dried in oven at 60 °C for 6 h. One gram of the washed cotton was taken and hydrolyzed in sulfuric acid solution (65%) (40 mL) at 72 °C for 30 min under magnetic stirring (800 rpm). The resulting solution was centrifuged for 5 min. The supernatant was decanted and the precipitate was recovered and re-dispersed in water. Centrifugation of the solution, followed by decantation of the supernatant and re-dispersion of the precipitate in fresh water, were repeated until the liquid phase became opaque. At this point, the liquid phase and the solid were sonicated for 6 h. The dispersion was centrifuged again at 5000 rpm for 5 min. The liquid phase was collected and the precipitate was discarded. The liquid phase was then centrifuged for 15 minutes at 12 000 rpm, resulting in the cellulose nanowhiskers.

Syntheses of amorphous carbon nanoneedles supported Co_3O_4 nanoparticles

The cellulose nanowhiskers obtained above were dispersed in 12 mL of water and 300 mL of absolute ethanol. Three different samples were prepared by adding different amounts of $Co(NO_3)_2$ into the above mixture. For sample A, 25 mg; for sample B, 75 mg; and for sample C, and 150 mg of $Co(NO_3)_2$ were stirred with the mixture for 30 min. After further addition of 5 mL of ammonia solution (25%), the dispersion was stirred for another 30 min. While the dispersion was kept stirring, 0.5 mL of tetraethyl orthosilicate was added into it. After stirring the dispersion for 12 h, the solid product was recovered by centrifugation and washed with ethanol and re-centrifuged. The precipitate was recovered, dried, and crushed in a mortar and pestle. The resulting powdered material (presumably containing Co_3O_4/CNN@SiO_2 core–shell nanoparticles) was thermally treated at different thermal stages as presented in Fig. S1.† The silica shells were etched off of the particles by stirring the material in 1 M aqueous NaOH solution for 2 h at 80 °C. The resulting solid (powdered) material was washed three times with water, *via* centrifugation at 12 000 rpm for 30 minutes, followed by decantation. It was then dried under ambient conditions, giving the desired Co_3O_4/CNN samples.

Acknowledgements

T.A. gratefully acknowledges the financial assistance provided to his group by the U.S. National Science Foundation (grants CBET-1134289, NSF-ACIF, and NSF Special Creativity grant in 2011).

Notes and references

1 V. Mazumder, Y. Lee and S. Sun, *Adv. Funct. Mater.*, 2010, **20**, 1224.
2 R. Silva and T. Asefa, *Adv. Mater.*, 2012, **24**, 1878.
3 Y. Zhao, L. Z. Fan, H. Z. Zhong, Y. F. Li and S. H. Yang, *Adv. Funct. Mater.*, 2007, **17**, 1537.
4 O. E. Herrera, D. P. Wilkinson and W. Merida, *J. Power Sources*, 2012, **198**, 132.
5 J. X. Wang, J. L. Zhang and R. R. Adzic, *J. Phys. Chem. A*, 2007, **111**, 12702.
6 J. K. Nørskov, J. Rossmeisl, A. Logadottir, L. Lindqvist, J. R. Kitchin, T. Bligaard and H. Jonsson, *J. Phys. Chem. B*, 2004, **108**, 17886.
7 Y. Q. Dong, H. C. Pang, H. B. Yang, J. Jiang, Y. W. Chi and T. Yu, *RSC Adv.*, 2014, **4**, 32791.
8 R. Silva, D. Voiry, M. Chhowalla and T. Asefa, *J. Am. Chem. Soc.*, 2013, **135**, 7823.
9 X. Zou, X. Huang, A. Goswami, R. Silva, B. R. Sathe, E. Mikmekova and T. Asefa, *Angew. Chem., Int. Ed.*, 2014, **53**, 4372.
10 K. P. Gong, F. Du, Z. H. Xia, M. Durstock and L. M. Dai, *Science*, 2009, **323**, 760.
11 P. M. Hallam, B. L. Riehl, B. D. Riehl and C. E. Bank, *RSC Adv.*, 2011, **1**, 93.
12 S. Guo, S. Zhang, L. Wu and S. Sun, *Angew. Chem., Int. Ed.*, 2012, **51**, 11770.
13 Y. Liang, Y. Li, H. Wang, J. Zhou, J. Wang, T. Regier and H. Dai, *Nat. Mater.*, 2011, **10**, 780.
14 Y. M. Tan, C. F. Xu, G. X. Chen, X. L. Fang, N. F. Zheng and Q. J. Xie, *Adv. Funct. Mater.*, 2012, **22**, 4584.
15 Y. Liang, H. Wang, P. Diao, W. Chang, G. Hong, Y. Li, M. Gong, L. Xie, J. Zhou, J. Wang, T. Z. Regier, F. Wei and H. Dai, *J. Am. Chem. Soc.*, 2012, **26**, 15849.
16 F. Zhang, F. M. Yasin, X. J. Chen, J. X. Mo, C. L. Raston, L. Colin and H. B. Zhang, *RSC Adv.*, 2013, **3**, 25166.
17 A. H. Castro Neto, F. Guinea, N. M. R. Peres, K. S. Novoselov and A. K. Geim, *Rev. Mod. Phys.*, 2009, **81**, 109.
18 X.-H. Guan, L. Yang, X. Guan and G.-S. Wang, *RSC Adv.*, 2015, **5**, 36185.
19 D. R. Dreyer, S. Park, C. W. Bielawski and R. S. Ruoff, *Chem. Soc. Rev.*, 2010, **39**, 228.
20 G. Eda, G. Fanchini and M. Chhowalla, *Nat. Nanotechnol.*, 2008, **3**, 270.
21 S. Kundu, T. C. Nagaiah, X. X. Chen, W. Xia, M. Bron, W. Schuhmann and M. Muhler, *Carbon*, 2012, **50**, 4534.
22 L. Li, Z. D. Wei, Y. Zhang, X. Q. Qi, M. R. Xia, J. Zhang, Z. G. Shao and C. X. Sun, *Sci. China, Ser. B: Chem.*, 2009, **52**, 571.
23 R. Silva, J. Al-Sharab and T. Asefa, *Angew. Chem., Int. Ed.*, 2012, **51**, 7171.
24 F. J. Maldonado-Hodar, C. Moreno-Castilla, J. Rivera-Utrilla, Y. Hanzawa and Y. Yamada, *Langmuir*, 2000, **16**, 4367.
25 P. Simon and A. Burke, *Electrochem. Soc. Interface*, 2008, **17**, 38.
26 S. Guo, S. Zhang, L. Wu and S. Sun, *Angew. Chem., Int. Ed.*, 2012, **51**, 11770.